Supplementary Information for
Additive Manufacturing of Self-Healing Elastomers

Kunhao Yu[1], An Xin[1], Haixu Du[1], Ying Li[2], Qiming Wang[1*]

[1]Sonny Astani Department of Civil and Environmental Engineering, University of Southern California, Los Angeles, CA 90089, USA
[2]Department of Mechanical Engineering and Institute of Materials Science, University of Connecticut, Storrs, CT 06269, USA
*Email: qimingw@usc.edu

1. Supplementary method: analytical modeling of disulfide-bond enabled self-healing

We develop a polymer-network based model to explain the experimentally measured self-healing behaviors of the created elastomer with disulfide bonds. This model is an extension of a model we recently developed for self-healing hydrogels crosslinked by nanoparticles[1]. We first model the constitutive behavior of the original elastomer and then model the interfacial self-healing behavior of the fractured elastomer.

1.1. Constitutive modeling of original elastomer

We assume that the elastomer is composed of *m* types of networks interpenetrating in the material bulk space (**Fig. S9**)[2]. The *i*th network is composed of the *i*th polymer chains with n_i Kuhn segment number. The length of the *i*th chain at the freely joint state is determined by the Kuhn segment number n_i as $r_i^0 = \sqrt{n_i}b$, where *b* is the Kuhn Segment length. Researchers usually denote the "chain length" as n_i[3]. Without loss of generality, the Kuhn segment number follows an order $n_1 \le n_2 ..... \le n_m$. We denote the number of *i*th chain per unit volume of material as N_i. Therefore, the total chain number per unit volume of material is $N = \sum_{i=1}^{m} N_i$. The chain number follows a statistical distribution as

$$P_i(n_i) = \frac{N_i}{N} \tag{S1}$$

The summation of the statistical distribution function is a unit, i.e., $\sum_{i=1}^{m} P_i = 1$. The chain-length distribution $P_i(n_i)$ is usually unknown without a careful experimental examination. Although researchers usually accept that the chain length is generally non-uniform[4], the most prevailing models for the rubber elasticity still consider the uniform chain length, such as three-chain model, four-chain model, and eight-chain model[3, 5, 6]. The consideration of non-uniform chain-length to model the elasticity behaviors of rubber-like materials was recently carried out by Wang et al. [2] and Vernerey et al.[7]. Because of the limited experimental technique to characterize the chain length distribution to date, the selection of chain-length distribution is still a little ambiguous. Wang et al. tested a number of chain-length distribution functions including uniform, Weibull, normal, and log-normal, and found that the log-normal distribution can best match the material's mechanical and mechanochemical behaviors [2]. In this paper, we simply employ the log-normal chain-length distribution, while other distributions may also work for our model. The log-normal chain-length distribution is written as

$$P_i(n_i) = \frac{1}{n_i \delta \sqrt{2\pi}} \exp\left[-\frac{(\ln n_i - \ln n_a)^2}{2\delta^2} \right] \tag{S2}$$

where n_a and δ are the mean of n_i and standard deviation of $\ln n_i$, respectively.

For the *i*th chain, if the end-to-end distance at the deformed state is r_i, the chain stretch is defined as $\Lambda_i = r_i / r_i^0$. The free energy of the deformed *i*th chain can be written as

$$w_i = n_i k_B T \left(\frac{\beta_i}{\tanh \beta_i} + \ln \frac{\beta_i}{\sinh \beta_i} \right) \tag{S3}$$

where k_B is the Boltzmann constant, T is the temperature in Kelvin, $\beta_i = L^{-1}\left(\Lambda_i / \sqrt{n_i}\right)$ and $L^{-1}(\ )$ is the inverse Langevin function. Considering the chain as an entropic spring, the force within the deformed *i*th chain can be written as

$$f_i = \frac{\partial w_i}{\partial r_i} = \frac{k_B T}{b} \beta_i \tag{S4}$$

To link the relationship between the macroscopic deformation at the material level and the microscopic deformation at the polymer chain level, we consider an interpenetrating model shown in **Fig. S9** [2]. We assume the *i*th chains assemble themselves into regular eight-chain structures[5]. We assume the material follows an affined deformation model[3, 6], so that the eight-chain structures deform by three principal stretches ($\lambda_1, \lambda_2, \lambda_3$) under the macroscopic deformation ($\lambda_1, \lambda_2, \lambda_3$) at the material level. Therefore, the stretch of each *i*th chain is

$$\Lambda_i = \sqrt{\frac{\lambda_1^2 + \lambda_2^2 + \lambda_3^2}{3}} \tag{S5}$$

At the undeformed state, the number of the *i*th chain per unit material volume is N_i. As the material is deformed, the active *i*th chain number decreases because the chain force promotes the dissociation of the dynamic bonds. We assume at the deformed state, the number of the active *i*th chain per unit material volume is N_i^a. Since every *i*th chain undergoes the same stretch Λ_i, the total free energy of the material per unit volume is

$$W = \sum_{i=1}^{m} N_i^a n_i k_B T \left(\frac{\beta_i}{\tanh \beta_i} + \ln \frac{\beta_i}{\sinh \beta_i} \right) \tag{S6}$$

where $\beta_i = L^{-1}\left(\Lambda_i / \sqrt{n_i}\right)$ and Λ_i is given in **Eq. S9**, and the active *i*th chain density N_i^a is obtained in the following sections.

We consider the material as incompressible and it is uniaxially stretched with three principal stretches ($\lambda_1 = \lambda, \lambda_2 = \lambda_3 = \lambda^{-1/2}$), the nominal stress along λ_1 direction can be calculated as

$$s_1 = \frac{\left(\lambda - \lambda^{-2}\right) k_B T}{\sqrt{3\lambda^2 + 6\lambda^{-1}}} \sum_{i=1}^{m} \left[N_i^a \sqrt{n_i} L^{-1}\left(\sqrt{\frac{\lambda^2 + 2\lambda^{-1}}{3n_i}} \right) \right] \tag{S7}$$

Next, we consider the association-dissociation kinetics of dynamic disulfide bonds (**Fig. S10**). We model the bond association and dissociation as a reversible chemical reaction[8, 9]. The forward reaction rate (from the associated state to the dissociated state) is k_i^f and reverse reaction rate is k_i^r. For simplicity, we assume that only two ends of a chain have ending groups for the dynamic bond [10]. If two end groups are associated, we consider this chain as "active"; otherwise, the chain is "inactive". The chemical reaction in **Fig. S10a** averagely involves one polymer chain; that is, the chemical reaction represents the transition between an active chain and an inactive chain. Here we denote the active *i*th chain per unit volume is N_i^a and the inactive *i*th chain per unit volume is N_i^d. The chemical kinetics can be written as

$$\frac{dN_i^a}{dt} = -k_i^f N_i^a + k_i^r N_i^d \tag{S8}$$

Since the total number of *i*th chain per unit volume defined as $N_i = N_i^a + N_i^d$, the chemical kinetics can be rewritten as

$$\frac{dN_i^a}{dt} = -\left(k_i^f + k_i^r\right) N_i^a + k_i^r N_i \tag{S9}$$

At the as-fabricated undeformed state, the reaction rates are $k_i^f = k_i^{f0}$ and $k_i^r = k_i^{r0}$, respectively. As the material is fabricated as an integrated solid, we simply assume the association reaction is much stronger than the dissociation reaction at the fabricated state, i.e., $k_i^{f0} \ll k_i^{r0}$. Otherwise, the polymer is unstable under external perturbations. Therefore, most of the *i*th chains are at the associated state, as the equilibrium value of N_i^a at the undeformed state is

$$N_i^a = \frac{k_i^{r0}}{k_i^{r0} + k_i^{f0}} N_i \approx N_i \tag{S10}$$

At the deformed state, the *i*th chain is deformed with stretch Λ_i. Since the bond strength of the dynamic bonds is much weaker than those of the permanent bonds such as covalent bonds, the chain force would significantly alter the bonding reaction [8, 9]. Specifically, the chain force tends to pull the bond open to the dissociated state. This point has been well characterized by Bell model for the ligand-receptor bonding for the cell adhesion behaviors, as well as for biopolymers [11]. We here employ a Bell-like model and consider the energy landscape between the associated state and dissociated state shown in **Fig. S10bc** [2]. We consider an energy barrier exists between the associated state (denoted as "A") and the dissociated state ("D") through a transition state ("T"). At the undeformed state of the *i*th chain, the energy barrier for $\mathrm{A} \to \mathrm{D}$ transition is ΔG^f and the energy barrier for $\mathrm{D} \to \mathrm{A}$ transition is ΔG^r (**Fig. S10b**). Under the deformed state of the *i*th chain, the chain force f_i lowers down the energy barrier of $\mathrm{A} \to \mathrm{D}$ transition to $\Delta G^f - f_i \Delta x$ and increases the energy barrier for $\mathrm{D} \to \mathrm{A}$ transition to $\Delta G^r + f_i \Delta x$, where Δx is the distance along the energy landscape coordinate (**Fig. S10c**). Since the occurrence of the chemical reaction

requires the overcoming of the energy barriers, the higher energy barrier is corresponding to the lower likelihood of the reaction. According to the Bell model, the reaction rates are governed by the energy barrier through exponential functions as [11, 12].

$$k_i^f = C_1 \exp\left(-\frac{\Delta G^f - f_i \Delta x}{k_B T}\right) = k_i^{f0} \exp\left(\frac{f_i \Delta x}{k_B T}\right) \tag{S11a}$$

$$k_i^r = C_2 \exp\left(-\frac{\Delta G^r + f_i \Delta x}{k_B T}\right) = k_i^{r0} \exp\left(-\frac{f_i \Delta x}{k_B T}\right) \tag{S11b}$$

Where C_1 and C_2 are constants and Δx is treated as a fitting parameter for the given material.

If the material is loaded with increasing stretch ($\lambda_1 = \lambda, \lambda_2 = \lambda_3 = \lambda^{-1/2}$) with a very small loading rate, the deformation of the material is assumed as quasi-static. It means that in every small increment of the load, the chemical reaction already reaches its equilibrium state with an equilibrium active *i*th chain number N_i^a . Under this condition, the active *i*th chain number per unit material volume is expressed as

$$N_i^a = \frac{N_i k_i^{r0} \exp\left(-\frac{f_i \Delta x}{k_B T}\right)}{k_i^{f0} \exp\left(\frac{f_i \Delta x}{k_B T}\right) + k_i^{r0} \exp\left(-\frac{f_i \Delta x}{k_B T}\right)} \tag{S12}$$

with the chain force f_i as expressed in **Eq. S4**.

In addition to the above association-dissociation kinetics, we also consider the effect of the network alteration[13, 14]. During the mechanical loading, a portion of dissociated short chains may reorganize to become active long chains[13, 14]. To capture this effect, we follow the network alteration theory to model the number of active chains to be an exponential function of the chain stretch Λ_i as

$$\frac{N_i^a}{N_i} = \exp\left[\alpha(\Lambda_i - 1)\right] \tag{S13}$$

where α is the chain alteration parameter. Similar network alteration model has been employed to model the chain reorganization for the Mullin's effect of rubber [13, 14], double-network hydrogels [15], and nanocomposite hydrogels [16]. It has been shown that the network alteration is a unique network damage mechanism that facilitates the stiffening effect of the stress-stretch curve [13, 14, 16]. Here, we harness this network alteration effect to better capture the stress-stretch curve shapes of the original elastomer.

1.2. Self-healing behavior of the fractured elastomer

We consider a self-healing elastomer sample shown in **Fig. S11**. We cut the sample into two parts and then immediately contact back. After a certain period of healing time *t*, the sample is uniaxially stretched until rupturing into two parts again. Here, we consider the self-healed sample is composed of two segments (**Fig. S11**): Around the healing interface, the polymer chain would diffuse across the interface to form new networks through forming new dynamic bonds. We call this region as "self-healed

segment". Away from the self-healed segment, the polymer networks are intact, and we call this region as "virgin segment".

As we assume in section 1.1, the *i*th chains form network following eight-chain structures (**Fig. S9**). For simplicity of analysis, we assume the cutting position is located at a quarter part of the eight chain cube, namely the center position between a corner and the center of the eight-chain cube (**Fig. S12a**). This assumption is just for the sake of symmetry to enable easy analysis. Other anti-symmetry cutting positions can also be analyzed using an averaging concept. The cutting process forces the polymer chains to be dissociated from the dynamic bond around the corner or center positions. Since we immediately contact the material back, we assume the ending groups of the dynamic bonds are still located around the cutting interface, yet without enough time to migrate into the material matrix (**Fig. S12b**)[1]. Driven by weak interactions between ending groups of the dynamic bonds, the ending groups on the interface will diffuse across the interface to penetrate into the matrix of the other part of the material to form new dynamic bonds. Specifically shown in **Fig. S12b**, the ending groups of the part A will penetrate into part B towards the center position of the cube, and the ending groups of part B will penetrate into Part A towards the corner positions of the cube. These interpenetration behaviors can be simplified as a 1D model shown in **Fig. S12c**. As shown in **Fig. S12c**, an open ending group around the interface penetrates into the other part of the material to find another open ending group to form a dynamic bond. Once the dynamic bond reforms, the initially "inactive" chain becomes "active". This behavior can be understood as two processes: chain diffusion and ending group reaction.

In the disulfide bond system shown in **Fig. 1c**, when we cut the material into two parts, the dissociated sulfide bonds undergo disulfide metathesis reactions (assisted by a catalyst tributylphosphine) to reform disulfide bonds around the interface. When the two material parts are brought into contact, these disulfide bonds will be mobilized by the catalyst tributylphosphine to move across the interface to exchange sulfide groups to form disulfide bonds to bridge the interface. Our generalized model shown in **Fig. S12** and discussed above can approximately capture the key physics of the healing behaviors of the disulfide bond system.

To model the chain diffusion, we consider a reptation-like model shown in **Fig. S12c** [3, 17-19]. We assume the polymer chain diffuses along its contour tube analogous to the motion of a snake. The motion of the polymer chain is enabled by extending out small segments called "minor chains". The curvilinear motion of the polymer chain is characterized by the Rouse friction model with the curvilinear diffusion coefficient of the *i*th chain written as

$$D_i = \frac{k_B T}{n_i \xi} \tag{S14}$$

where ξ is the Rose friction coefficient per unit Kuhn segment.

We note that the chain motion follows a curvilinear path; therefore, we construct two coordinate systems *s* and *y*, where *s* denotes the curvilinear path along the minor chains and *y* denotes the linear path from the interface to the other open ending group. When the *i*th chain moves s_i distance along the curvilinear path, it is corresponding to y_i distance along *y* coordinate. Here we assume the selection of the

curvilinear path is fully stochastic following the Gaussian statistics[20-22]. Therefore, the conversion of the distances in two coordinate systems is expressed as

$$y_i = \sqrt{s_i b} \tag{S15}$$

According to the eight-chain cube assumption, the distance between the corner and the center within the *i*th network cube at its freely joint state is

$$L_i \approx \sqrt{n_i} b \tag{S16}$$

The distance between the ending group around the interface and the other ending group in the matrix is $L_i/2$. According to **Eq. S15**, the positions $y = 0$ and $y = L_i/2$ are corresponding to $s = 0$ and $s = L_i^2/4b$, respectively.

If we only consider the polymer chain diffusion, the diffusion of the *i*th chain can be modeled with the following diffusion equation along the curvilinear coordinate *s*,

$$\frac{\partial C_i^d(t,s)}{\partial t} = D_i \frac{\partial^2 C_i^d(t,s)}{\partial s^2} \tag{S17}$$

where $C_i^d(t,s)$ is the inactive *i*th chain number per unit length (with the unit area) along the coordinate *s* ($0 \le s \le L_i^2/4b$) at time *t*. However, the chain behavior is more complicated than just diffusion, because during the diffusion the ending group would encounter another ending group to undergo a chemical reaction to form a new dynamic bond. Although the chemical reaction may only occur around the ending group (relatively immobile ending group at $s = L_i^2/4b$), the reaction forms dynamic bonds to transit an inactive chain into an active chain, and this reaction would reduce the amount of the inactive ending groups and further drive the motion of the other inactive ending groups. Therefore, the chain diffusion and ending group reaction actually are strongly coupled. Therefore, we consider an effective diffusion-reaction model to consider the effective behaviors of the chain and the ending group as [23]

$$\frac{\partial C_i^d(t,s)}{\partial t} = D_i \frac{\partial^2 C_i^d(t,s)}{\partial s^2} - \frac{\partial C_i^a(t,s)}{\partial t} \tag{S18}$$

$$\frac{\partial C_i^a(t,s)}{\partial t} = k_i^{r0} C_i^d(t,s) - k_i^{f0} C_i^a(t,s) \tag{S19}$$

where $C_i^a(t,s)$ is the active *i*th chain number per unit length (with the unit area) along the coordinate *s* ($0 \le s \le L_i^2/4b$) at time *t*. As the polymer chain is freely joint during the diffusion process, we here use the chemical reaction rates k_i^{f0} and k_i^{r0}.

In the initial state of the self-healing, all mobile open-ending groups of the *i*th chains are located around the healing interface. Therefore, the initial condition of the diffusion-reaction model is

$$C_i^d(t=0,s) = N_i \delta(s) \tag{S20}$$

$$C_i^a(t=0,s)=0 \tag{S21}$$

where $\int_{-\infty}^{\infty}\delta(s)ds=1$.

For a self-healing polymer that is capable of forming a stable solid form and enabling relatively short healing time, the basic requirement is $k_i^{f0}<k_i^{r0}$. Here, we further focus our attention on polymers with good healing capability, so that the polymers can easily self-heal under relatively mild conditions. This requirement further implies that k_i^{r0} should be much larger than k_i^{f0}, i.e., $k_i^{r0}>>k_i^{f0}$. Under this condition, **Eqs. S18-S19** can be reduced as

$$\frac{\partial C_i^d(t,s)}{\partial t}=D_i\frac{\partial^2 C_i^d(t,s)}{\partial s^2}-k_i^{r0}C_i^d(t,s) \tag{S22}$$

At the same time, around the location $s=L_i^2/4b$, all open ending groups form dynamic bonds. This leads to the vanishing of inactive chains around the location $s=L_i^2/4b$, written as

$$C_i^d\left(t,s=L_i^2/4b\right)=0 \tag{S23}$$

Along with above initial and boundary conditions, the reaction-diffusion equation (**Eq. S22**) can be solved analytically or numerically. Once $C_i^d(t,s)$ in the diffusion-reaction model is solved, we can further obtain the active *i*th chain number per unit volume of the self-healing segment at healing time *t*, written as

$$\frac{N_i^h(t)}{N_i}=1-\frac{4b}{L_i^2}\int_0^{L_i^2/4b}\frac{C_i^d(t,s)}{N_i}ds \tag{S24}$$

where $N_i^h(t)$ is for the self-healed segment at the undeformed state ($\lambda_1=\lambda_2=\lambda_3=1$), and the superscript "*h*" denotes "healed".

At the deformed state, the active *i*th chain number in the self-healed segment decreases with the increasing stretch. If we consider a quasistatic load with principal stretches ($\lambda_1=\lambda^h,\lambda_2=\lambda_3=\left(\lambda^h\right)^{-1/2}$), the active *i*th chain number per unit volume of the self-healing segment can be calculated as

$$N_i^{ah}(t)=\frac{N_i^h(t)k_i^{r0}\exp\left(-\frac{f_i\Delta x}{k_BT}\right)}{k_i^{f0}\exp\left(\frac{f_i\Delta x}{k_BT}\right)+k_i^{r0}\exp\left(-\frac{f_i\Delta x}{k_BT}\right)} \tag{S25}$$

with the chain force expressed as

$$f_i = \frac{k_B T}{b} L^{-1}\left(\sqrt{\frac{\left(\lambda^h\right)^2 + 2\left(\lambda^h\right)^{-1}}{3n_i}}\right) \tag{S26}$$

Therefore, the free energy per unit volume of the self-healed segment can be written as

$$W^h = \sum_{i=1}^{m} N_i^{ah}(t) n_i k_B T\left(\frac{\beta_i^h}{\tanh \beta_i^h} + \ln \frac{\beta_i^h}{\sinh \beta_i^h}\right) \tag{S27}$$

where $\beta_i^h = L^{-1}\left(\sqrt{\left[\left(\lambda^h\right)^2 + 2\left(\lambda^h\right)^{-1}\right]/3n_i}\right)$ and $N_i^{ah}(t)$ is given by **Eq. S25**. The nominal stress along λ_1 direction can be written as

$$s_1^h\left(\lambda^h, t\right) = \frac{\left(\lambda^h - \lambda^{h^{-2}}\right) k_B T}{\sqrt{3\left(\lambda^h\right)^2 + 6\left(\lambda^h\right)^{-1}}} \sum_{i=1}^{m}\left[N_i^{ah}(t)\sqrt{n_i} L^{-1}\left(\sqrt{\frac{\left(\lambda^h\right)^2 + 2\left(\lambda^h\right)^{-1}}{3n_i}}\right)\right] \tag{S28}$$

where t is the healing time and λ^h is the uniaxial stretch in the self-healed segment.

We consider a self-healed sample (length H) with a self-healed segment (length H^h, $H^h \ll H$) and two virgin segments (**Fig. S11**). Under a uniaxial stretch, the lengths of the whole sample and the self-healed segment become h and h^h, respectively. The stretch of the self-healed segment is $\lambda^h = h^h / H^h$. The stretch of the virgin segment is approximately equal to the stretch of the whole sample λ because $\lambda = h/H \approx \left(h - h^h\right)/\left(H - H^h\right)$. We assume the initial cross-sections of the virgin segment and the self-healed segment are the same; then, the uniaxial nominal stresses in the self-healed segment and the virgin segment should be equal, written as

$$s_1^h\left(\lambda^h\right) = s_1(\lambda) \tag{S29}$$

where $s_1^h\left(\lambda^h\right)$ is referred to **Eq. S28**, and $s_1(\lambda)$ is referred to **Eq. S7**. From **Eq. S29**, we can determine the stress-stretch behaviors of the self-healed sample for various healing time t.

The comparisons between the experimentally measured self-healing behaviors of the studied elastomers and theoretically calculated results are shown in **Fig. S13**. We employ an inhomogeneous chain-length distribution shown in **Fig. S13a**. The employed parameters are shown in **Table S1**. The chain dynamics parameters and Rouse friction coefficients are within the reasonable order compared with limited experimental or simulation results in the references [1, 21, 24, 25]. The theoretically calculated stress-strain curves can consistently match the experimentally measured results (**Fig. S13b**). In addition, the theoretically calculated relationships between the healing strength ratio and the healing time also agree well with the experimental results (e.g., 60°C in **Fig. S13c**).

1.3. Effect of temperature on the self-healing behavior

The temperature term is directly involved in the expression of the nominal stress of the original hydrogel and self-healed hydrogel shown in **Eqs. S7** and **S27**. However, the existence of both expressions results in the vanishing of the temperature term in the healing strength ratio. Here, we more focus on the effects of temperatures on the Rouse friction coefficient (**Eq. S13**). The curvilinear diffusivity can be affected by the temperature from two aspects: First, the temperature term explicitly appears in **Eq. S13** through k_BT. Then, the Rouse friction coefficient ξ monotonically decreases with increasing temperature [3]. This behavior can usually be modeled by Vogel relationship as [3, 21, 26],

$$\xi \propto \exp\left(\frac{B}{T - T_\infty} - A\right) \tag{S30}$$

where T_∞ is the Vogel temperature, B (positive) and A are constant parameters. By judiciously selecting these three parameters, we can quantitatively reveal the relationship between the temperature and self-healing strength ratio. Using $T_\infty = 383.2K$, $B = 486.5K$ and $A = -5.96$, we are able to theoretically capture the relationships between the healing strength ratio and the healing time, which show good agreement with experimental results for various temperatures from 40°C to 60°C (**Fig. S13c**). We further define the equilibrium healing time as the healing time corresponding to 90% healing strength ratio. We find out that the theoretically calculated relationship between the equilibrium healing time and the healing temperature is consistent with the experimental result (**Fig. S13d**).

2. Supplementary table

Table S1. Model parameters used in this paper.

Parameter	Definition	Value
k_i^{f0} (s^{-1})	Forward reaction rate	$2x10^{-7}$
k_i^{r0} (s^{-1})	Reverse reaction rate	$4x10^{-4}$
Δx (m)	The distance along the energy landscape coordinate	$1.2x10^{-9}$
b (m)	Kuhn segment length	$2x10^{-10}$
n_1	Minimum chain length	10
n_m	Maximum chain length	120
n_a	Average chain length	49
δ	Chain length distribution width	0.18
α	Chain alteration parameter	0.5
ξ (N/m)	Rouse friction coefficient	$2.4x10^{-6}$ for 60°C
T_∞ (K)	Vogel temperature	383.2
B (K)	Parameter for the Vogel relationship	486.5
A	Parameter for the Vogel relationship	-5.96

3. Supplementary figures

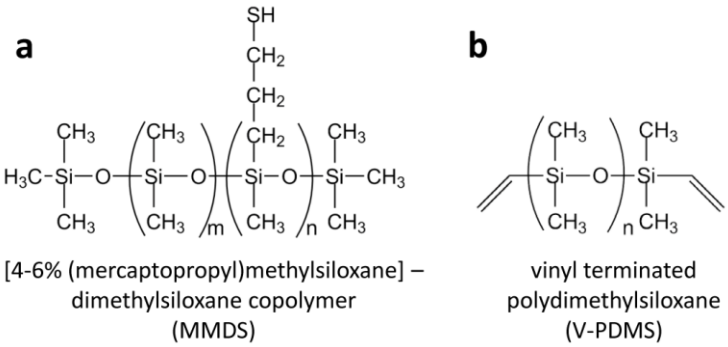

Figure S1. Chemical Structures of (a) MMDS and (b) V-PDMS.

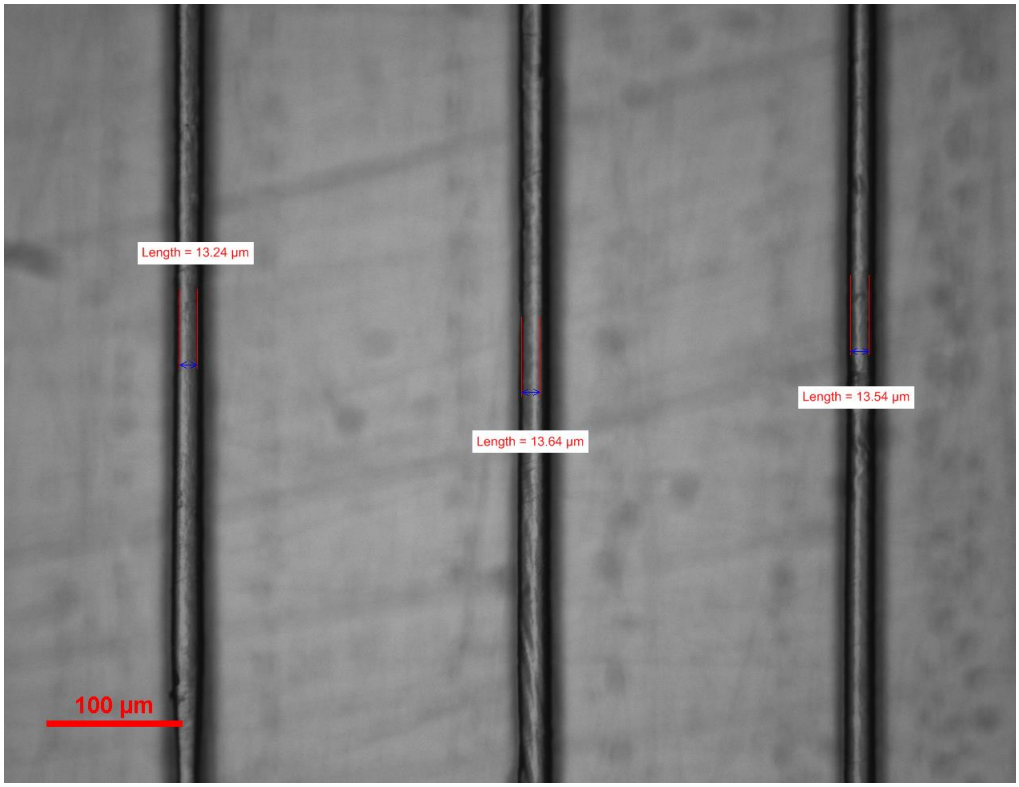

Figure S2. Microscopic image to show the manufacturing resolution. The image is taken using a Nikon microscope (Eclipse LV100ND).

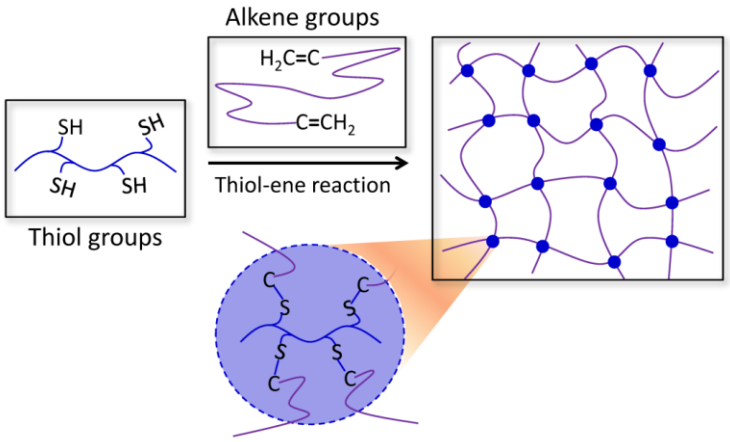

Figure S3. Molecular design of the control elastomer. MMDS and V-PDMS directly have a thiol-ene photopolymerization reaction to form an elastomer network without disulfide bonds.

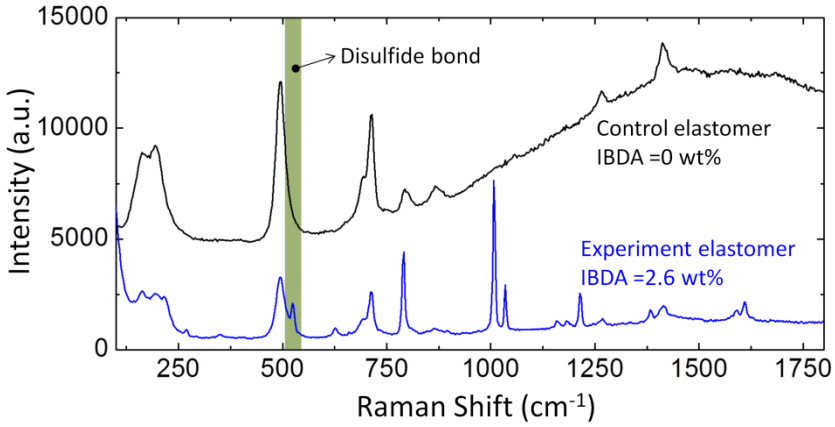

Figure S4. Raman spectra of the control elastomer (No IBDA) and the experiment elastomer (IBDA concentration 2.6wt%). The new band ~520 cm^{-1} is corresponding to the disulfide bond.

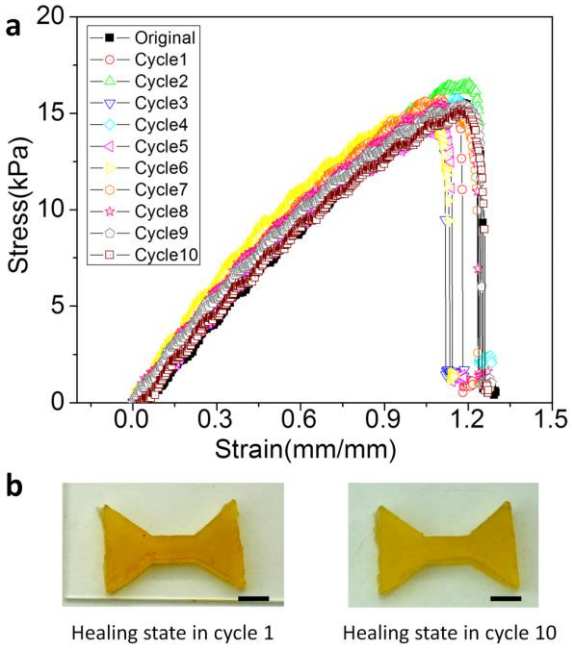

Figure S5. (a) Nominal stress-strain curves of the self-healed experiment elastomer samples after various healing cycle (each 2 h at 60°C). (b) The experiment elastomer sample at the healing state of cycles 1 ad 10. The sample does not shrink after the 10-cycle healing process. The scale bar represents 5 mm.

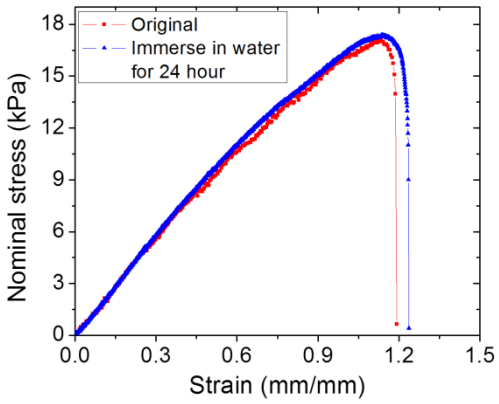

Figure S6. Nominal stress-strain curves of original experiment elastomer and the elastomer after being immersed in DI water for 24 h.

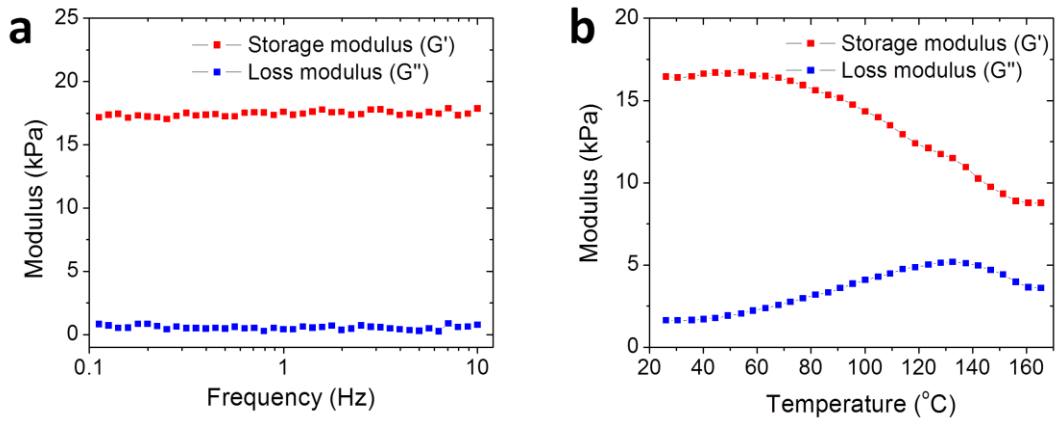

Figure S7. (a) The storage and loss moduli of the experiment elastomer over frequency 0.1-10 Hz in a frequency sweep test. (b) The storage and loss moduli of the experiment elastomer over temperature 25-165°C in a frequency sweep test with frequency 1 Hz.

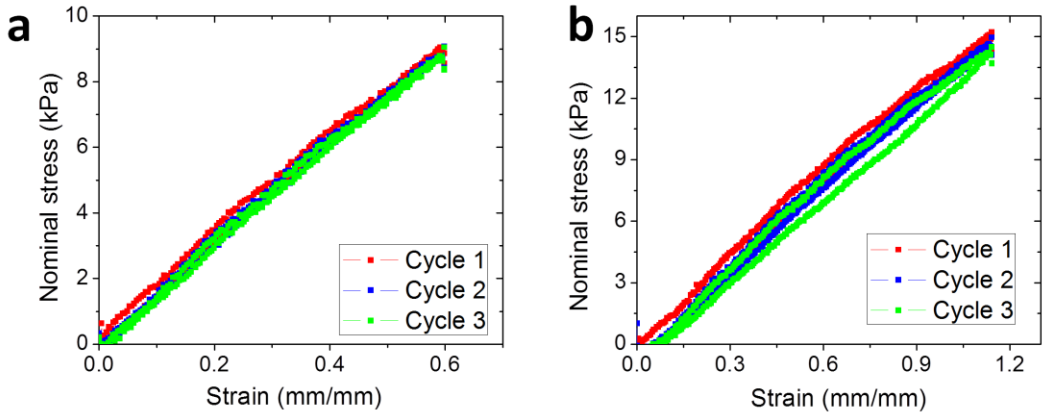

Figure S8. Nominal stress-strain curves of the experiment elastomer over three sequential tensile loading-unloading cycles with the maximal strain at (a) 0.6 mm/mm and (b) 1.1 mm/mm.

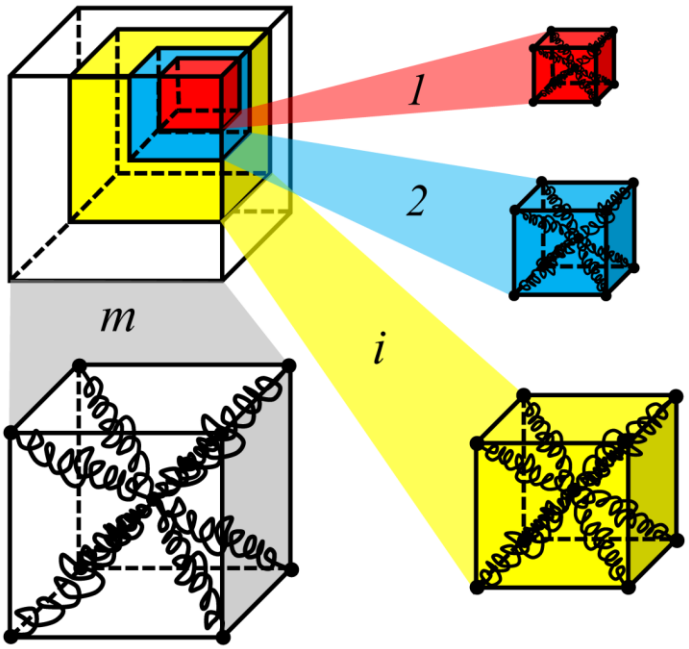

Figure S9. Schematics to illustrate an interpenetrating network model. *m* types of networks interpenetrate in the material bulk space. The *i*th network is composed of the *i*th polymer chains with Kuhn segment number n_i ($1 \le i \le m$). Each type of polymer chain self-organizes into eight-chain structures.

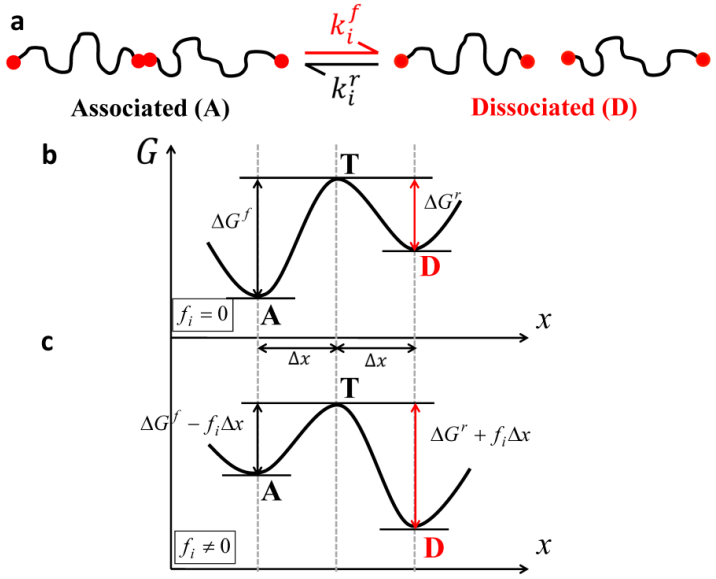

Figure S10. (a) Schematic to show the association-dissociation kinetics of the dynamic bond on the *i*th chain. We consider the reaction from the associated state to the dissociated state as the forward reaction of the *i*th chain with reaction rate k_i^f $(1 \le i \le m)$, and corresponding reaction from the dissociated state to the associated state as the reverse reaction with reaction rate k_i^r. (bc) Potential energy landscape of the reverse reaction of the dynamic bond on the *i*th chain with chain force (b) $f_i = 0$ and (c) $f_i \neq 0$. "A" stands for the associated state, "D" stands for the dissociated state, and "T" stands for the transition state.

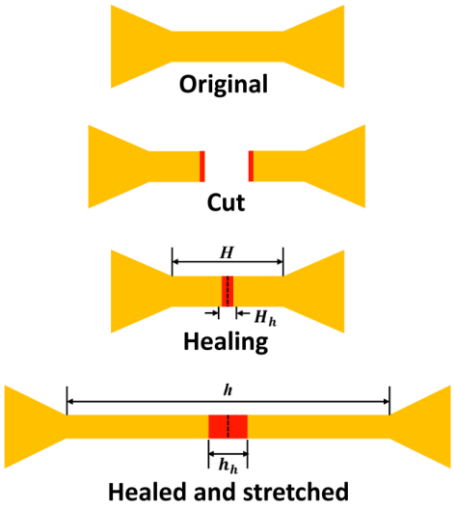

Figure S11. A schematic to show the self-healing process.

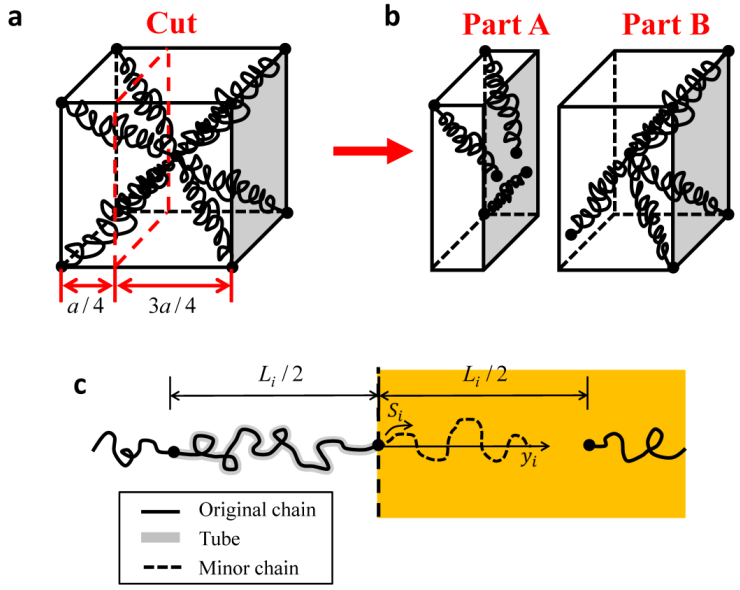

Figure S12. (a, b) Schematics of the eight-chain network model before and after the cutting process. The cutting is assumed to be located in a quarter position of the cube. (c) A schematic to show the diffusion behavior of the *i*th polymer chain across the interface.

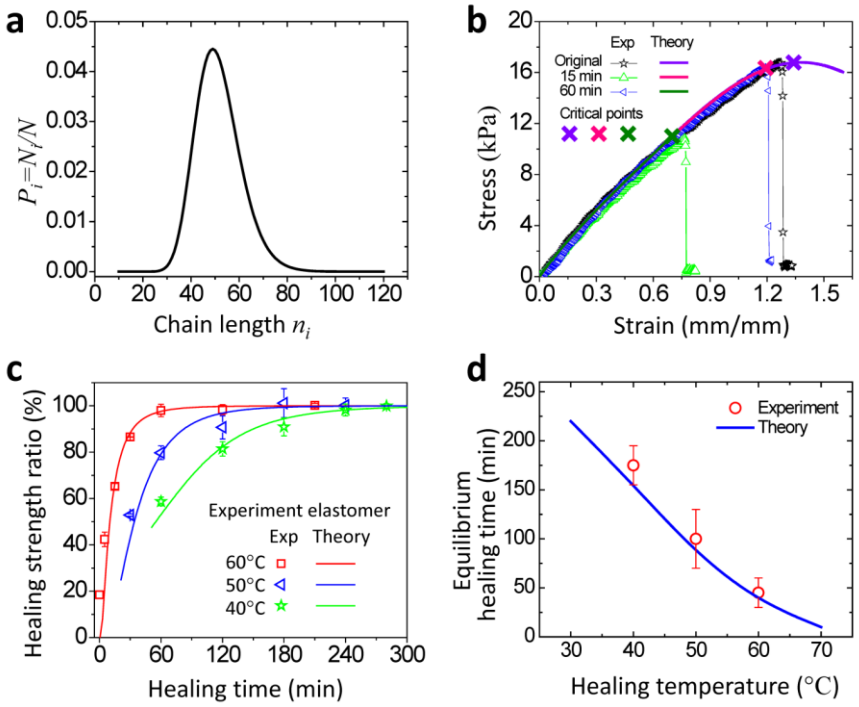

Figure S13. (a) Chain length distribution of the self-healing elastomer network. (b) The experimentally measured and theoretically calculated (b) stress-stretch curves of the original and self-healed elastomer samples, (c) healing strength ratios as a function of the healing time for various healing temperatures, and (d) the equilibrium healing time as a function of the healing temperature. The equilibrium healing time is defined as the healing time corresponding to 90% healing strength ratio.

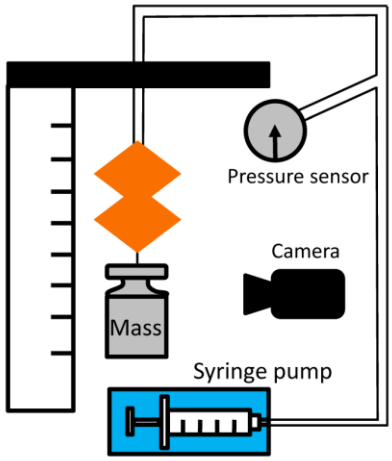

Figure S14. Experimental setup for the self-healing 3D soft actuator.

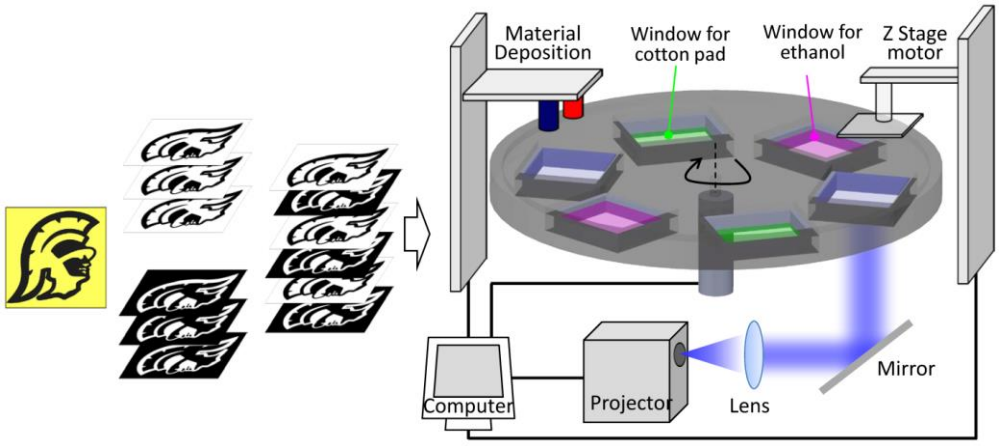

Figure S15. Schematics to show the experimental setup of the multimaterial stereolithography system.

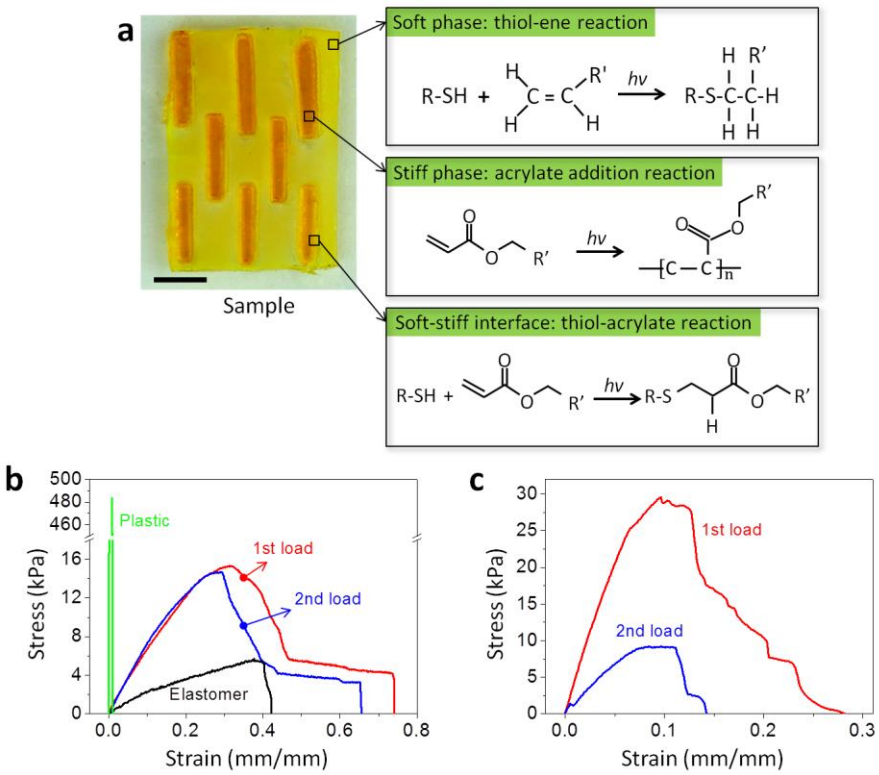

Figure S16. (a) The fabricated sample of the nacre-like stiff-soft composite. During the AM process, the soft phase undergoes a thiol-ene reaction, the stiff phase acrylate addition reaction, and the soft-stiff interface thiol-acrylate reaction. "*hv*" represents the light exposure. The scale bar represents 3 mm. (b) The uniaxial nominal stress-strain curves of the original experiment composite (1st load), the self-healed experiment composite (2nd load), pure HDDA, and pure self-healable elastomer. (c) The uniaxial nominal stress-strain curves of the original control composite (1st load) and the self-healed control composite (2nd load).

Reference

1. Wang Q, Gao Z, Yu K. Interfacial self-healing of nanocomposite hydrogels: Theory and experiment. *J. Mech. Phys. Solids.* **109**, 288-306 (2017).
2. Wang Q, Gossweiler GR, Craig SL, Zhao X. Mechanics of mechanochemically responsive elastomers. *Journal of the Mechanics and Physics of Solids* **82**, 320-344 (2015).
3. Rubinstein M, Colby R. *Polymer Physics*. Oxford University Press (2003).
4. Erman B, Mark JE. *Structures and properties of rubberlike networks*. Oxford University Press (1997).
5. Arruda EM, Boyce MC. A three-dimensional constitutive model for the large stretch behavior of rubber elastic materials. *Journal of the Mechanics and Physics of Solids* **41**, 389-412 (1993).
6. Treloar LRG. *The physics of rubber elasticity*. Oxford University Press (1975).
7. Vernerey FJ, Long R, Brighenti R. A statistically-based continuum theory for polymers with transient networks. *Journal of the Mechanics and Physics of Solids* **107**, 1-20 (2017).
8. Kramers HA. Brownian motion in a field of force and the diffusion model of chemical reactions. *Physica* **7**, 284-304 (1940).
9. Hänggi P, Talkner P, Borkovec M. Reaction-rate theory: fifty years after Kramers. *Reviews of Modern Physics* **62**, 251 (1990).
10. Stukalin EB, Cai L-H, Kumar NA, Leibler L, Rubinstein M. Self-healing of unentangled polymer networks with reversible bonds. *Macromolecules* **46**, 7525-7541 (2013).
11. Bell GI. Models for the specific adhesion of cells to cells. *Science* **200**, 618-627 (1978).
12. Ribas-Arino J, Marx D. Covalent mechanochemistry: theoretical concepts and computational tools with applications to molecular nanomechanics. *Chemical reviews* **112**, 5412-5487 (2012).
13. Marckmann G, Verron E, Gornet L, Chagnon G, Charrier P, Fort P. A theory of network alteration for the Mullins effect. *J. Mech. Phys. Solids.* **50**, 2011-2028 (2002).
14. Chagnon G, Verron E, Marckmann G, Gornet L. Development of new constitutive equations for the Mullins effect in rubber using the network alteration theory. *International Journal of Solids and Structures* **43**, 6817-6831 (2006).
15. Zhao X. A theory for large deformation and damage of interpenetrating polymer networks. *Journal of the Mechanics and Physics of Solids* **60**, 319-332 (2012).
16. Wang Q, Gao Z. A constitutive model of nanocomposite hydrogels with nanoparticle crosslinkers. *Journal of the Mechanics and Physics of Solids* **94**, 127-147 (2016).
17. de Gennes PG. Reptation of a Polymer Chain in the Presence of Fixed Obstacles. *Journal of Chemical Physics* **55**, 572-579 (1971).
18. Doi M, Edwards SF. Dynamics of concentrated polymer systems. Part 1.-Brownian motion in the equilibrium state. *J. Chem. Soc., Faraday Trans.* **74**, 1789-1801 (1978).
19. De Gennes P-G. *Scaling concepts in polymer physics*. Cornell university press (1979).
20. Kim YH, Wool RP. A theory of healing at a polymer-polymer interface. *Macromolecules* **16**, 1115-1120 (1983).
21. Whitlow SJ, Wool RP. Diffusion of polymers at interfaces: a secondary ion mass spectroscopy study. *Macromolecules* **24**, 5926-5938 (1991).
22. Zhang H, Wool RP. Concentration profile for a polymer-polymer interface. 1. Identical chemical composition and molecular weight. *Macromolecules* **22**, 3018-3021 (1989).
23. Crank J. *The mathematics of diffusion*. Oxford university press (1979).
24. Chapman BR, *et al.* Structure and dynamics of disordered tetrablock copolymers: composition and temperature dependence of local friction. *Macromolecules* **31**, 4562-4573 (1998).
25. Silberstein MN, *et al.* Modeling mechanophore activation within a viscous rubbery network. *Journal of the Mechanics and Physics of Solids* **63**, 141-153 (2014).
26. Wool RP. Self-healing materials: a review. *Soft Matter* **4**, 400-418 (2008).